

# Enhancement of damping in a turbulent atomic Bose-Einstein condensate

Junghoon Lee,<sup>1</sup> Jongmin Kim,<sup>1</sup> Jongheum Jung,<sup>1</sup> and Y. Shin<sup>1,2,\*</sup>

<sup>1</sup>*Department of Physics and Astronomy, Seoul National University, Seoul 08826, Korea*

<sup>2</sup>*Institute of Applied Physics, Seoul National University, Seoul 08826, Korea*

(Dated: February 12, 2025)

We investigate the collective oscillations of atomic Bose-Einstein condensates (BECs) containing spin-superflow turbulence and observe an enhancement in damping due to the turbulence. As steady-state turbulence is maintained in a spin-1 BEC using a spin-driving technique, we measure the damping rate of the quadrupole oscillation of the BEC across a range of temperatures and show that it exceeds the thermal damping rate predicted by a Landau damping model for BECs without turbulence. To explain the additional damping, we introduce an effective viscosity  $\nu_T$ , analogous to the turbulent viscosity in classical turbulence. Our measurements suggest that  $\nu_T \sim 0.05 \times \frac{h}{m}$ , where  $h$  is Planck's constant and  $m$  is the atomic mass.

Turbulent or eddy viscosity is a phenomenological concept used to model the effects of turbulence on momentum transport within a fluid [1, 11]. This form of viscosity differs from the molecular viscosity in a laminar flow and originates from the macroscopic turbulent eddies that prevail in chaotic fluid motions. The eddies interact dynamically across a wide range of length scales, thereby facilitating enhanced momentum exchanges and mixing within the fluid. Although turbulent viscosity, being an isotropic scalar quantity, appears too simplistic to capture the intricate dynamics of turbulent flows, it has nevertheless served as an effective and remarkably useful framework for predicting complex flow behaviors in various practical applications, from aerospace engineering [3, 4] to ventilation in built environments [5].

An interesting question is whether the notion of turbulent viscosity can be extended to superfluids, which have zero intrinsic viscosity and behave differently from classical fluids due to quantum effects. Although inviscid, superfluids can dissipate kinetic energy via the dynamics of quantum vortices and their interactions with the co-existing normal fluid component [6–10]. Energy cascades and Kolmogorov scaling behaviors have been observed in turbulent superfluids [11, 12], indicating a remarkable similarity to classical fluids. Previously, the concept of eddy viscosity was adopted in work of turbulence in superfluid helium to account for the excess pressure gradient observed under heat counterflow conditions [13, 14], but the interpretation remains inconclusive due to uncertainties regarding the homogeneity of the turbulence and ambiguities in the normal fluid state [15]. Recent piston-driven shock experiments in atomic Bose-Einstein condensates (BECs) recalled eddy viscosity to explain dissipative shock dynamics [16]. A coherent understanding of turbulent viscosity in superfluid turbulence at the macroscopic level is highly desirable and may have implications for astrophysics, particularly in the context of neutron stars with superfluid interiors [17, 18].

In this paper, we present an experimental investigation of the viscous effects of turbulence in atomic BECs. We generate a spin-1 BEC in a non-equilibrium steady state

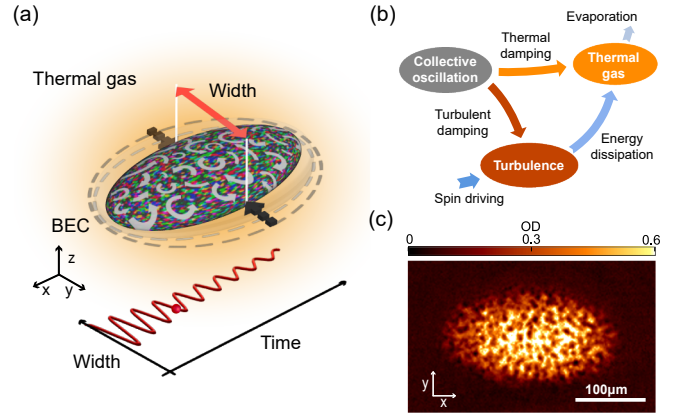


FIG. 1. Collective oscillations of a turbulent Bose-Einstein condensate (BEC). (a) Schematic of the experiment. A BEC with internal turbulent flow (gray arrows) is confined in a harmonic potential and undergoes shape oscillations that are damped by the thermal background gas. The turbulence is sustained by resonant rf spin driving, which steadily generates an irregular spin texture (color pattern). (b) Energy flow diagram illustrating two pathways for dissipation of collective excitation energy: direct interaction with thermal components and energy transfer into the internal turbulence. (c) Image of a turbulent BEC after an 18-ms time-of-flight.

characterized with a turbulent spin-superflow [3, 4, 7, 22] and examine the impact of turbulence on the damping of collective quadrupole oscillations of the BEC. By comparing systems with and without turbulence, and measuring the temperature dependence of the damping rates, we reveal that turbulent BECs exhibit enhanced damping beyond the theoretical predictions for thermal Landau damping [23, 24]. Using a classical turbulence framework [12, 25], we introduce a turbulent kinematic viscosity,  $\nu_T$ , to explain the additional damping observed, and our results suggest that  $\nu_T \sim 0.05 \times h/m$  with  $h$  being Planck's constant and  $m$  the atomic mass. This work opens new avenues for the experimental studies of the hydrodynamic properties of superfluid turbulence, using atomic BECs with steady-state turbulence.

Our superfluid system is a BEC of  $^{23}\text{Na}$  atoms in the  $F=1$  hyperfine state, which has internal spin degrees of freedom [2, 8]. A BEC is prepared initially in the  $m_F = -1$  state in an optical dipole trap under a uniform external magnetic field. Turbulence is generated using a spin-driving technique [3, 7], where a radio-frequency (RF) magnetic field is applied with an oscillating frequency set to the Larmor frequency. Due to chaotic spin dynamics under resonant spin driving [4–6], a non-equilibrium steady state emerges with an irregular spin texture, leading to turbulent superflow in the BEC system [Fig. 1(c)]. We emphasize that the driving occurs at the spin energy scale ( $\varepsilon_s/h \sim 50$  Hz), negligibly small compared to the chemical potential ( $\mu/h \sim 1$  kHz) such that the turbulent state is sustained under driving without significant heating. The lifetime of the sample in the non-equilibrium steady state exceeds 30 s, which allows an investigation of the collective oscillations of the turbulent BEC [31, 32].

Collective oscillations of a trapped BEC typically undergo damping in the presence of a coexisting thermal cloud. Thermal dissipation is well described by the Landau damping process, where the energy and momentum of collective excitations are absorbed by thermally excited particles [23, 24]. For a BEC with turbulence, an additional damping mechanism can arise from the nonlinear mixing effect induced by turbulence [Fig. 1(b)], which diffuses the long-wavelength momentum of the collective excitations within the BEC. Energy transport in momentum space has been demonstrated in a recent experiment with turbulent atomic BECs [12].

We excite the oscillations of the BEC by periodically modulating the depth of the optical trap as  $U(t) = U_f[1 + \epsilon \sin(\omega_d t)]$  with frequency  $\omega_d$  and relative amplitude  $\epsilon$ . For our highly oblate sample with trapping frequencies  $(\omega_x, \omega_y, \omega_z) = 2\pi \times (7.5, 15.3, 730)$  Hz, two distinct quadrupole modes are identified with oscillation frequencies of about 11 Hz and 25 Hz, respectively. The high (low) frequency mode exhibits in-phase (out-of-phase) oscillations in condensate widths along the  $x$  and  $y$  directions [9, 10]. In the present work, we investigate a high-frequency mode in which the BEC experiences a higher shear flow during oscillations, thus offering a favorable setting for exploring turbulent viscosity [35].

We characterize the collective excitation mode by measuring the steady-state response of the BEC to trap modulations as a function of the modulation frequency  $\omega_d$ . After a time of  $t_0 = 50 \frac{2\pi}{\omega_d}$ , ensuring that the BEC oscillations reach a quasi-steady state, the normalized width  $\tilde{W}(t)$  of the BEC along the  $y$  direction is tracked by taking a time-of-flight image of the sample for various driving times  $t$ . Here,  $\tilde{W} = W/W_{\text{eq}}$ , with  $W$  being the measured width and  $W_{\text{eq}}$  the width of an unmodulated BEC for the same atom number  $N_c$ . The relative amplitude  $A$  and phase  $\phi$  of the BEC oscillations are determined from the fit of  $\tilde{W}(t) = 1 + \alpha_\tau A \sin(\omega_d t + \phi + \varphi_\tau)$  to the

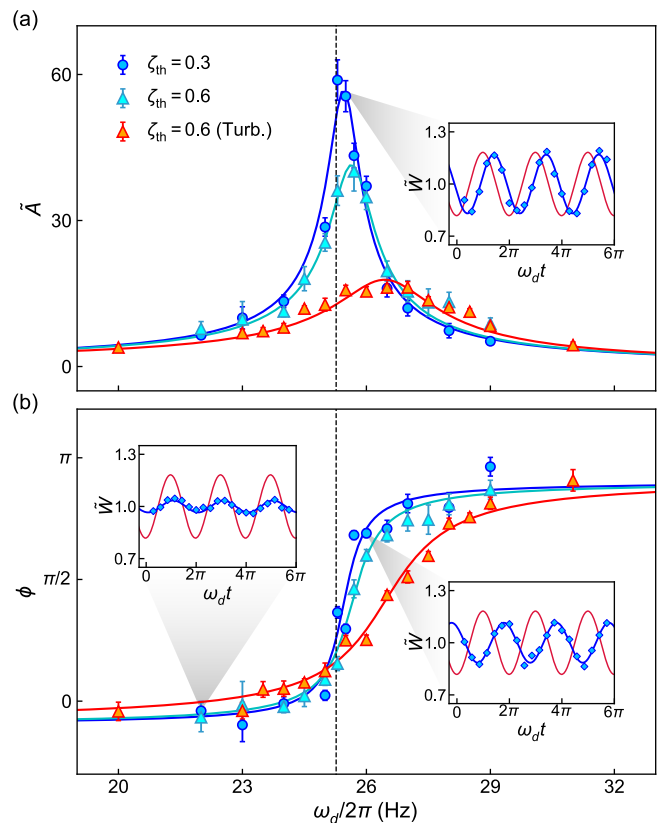


FIG. 2. Responses of BECs to the periodic modulations of the trapping potential. (a) Amplitude magnification factor  $\tilde{A}$  and (b) relative phases  $\phi$  of the shape oscillations of the driven BECs as functions of the driving frequency  $\omega_d$  for three different samples: ordinary single-component samples with thermal fractions  $\zeta_{\text{th}} = 0.3$  (blue) and  $= 0.6$  (cyan), and a turbulent BEC sample with  $\zeta_{\text{th}} = 0.6$  (orange). The solid lines represent indicative Lorentzian curves in (a) and arctangent functions with offsets in (b) fitted to the corresponding data sets (see text). The dashed vertical lines indicate the resonant frequency of the quadrupole oscillation, estimated from the trapping frequencies. The insets show the time evolution of the normalized condensate width  $\tilde{W}$  in the sample with  $\zeta_{\text{th}} = 0.3$  for three different values of  $\omega_d$ . The red lines denote guides for oscillations in phase with the trap modulations.

data, where  $\alpha_\tau = \sqrt{1 + (\omega_d \tau)^2}$  and  $\varphi_\tau = \tan^{-1}(\omega_d \tau)$  account for the effects of amplitude amplification and the phase change, respectively, due to time-of-flight expansion ( $\tau = 18$  ms) [35]. In the measurement, the magnitude of the trap modulations was adjusted to hold  $A$  to less than 10%, resulting in  $\epsilon \leq 1.5\%$ . Because  $W_{\text{eq}} \propto U_f^{-1/5}$  in a harmonic potential, the change in width at equilibrium is  $\Delta W_{\text{eq}} = \frac{1}{5}\epsilon W_{\text{eq}}$  for a small  $\epsilon$ , and we estimate the amplitude magnification factor for the driven oscillations as  $\tilde{A} = 5A/\epsilon$ .

In Fig. 2, we present the response spectra  $\tilde{A}(\omega_d)$  and  $\phi(\omega_d)$  for three different samples, in this case BECs with the thermal fraction  $\zeta_{\text{th}} = 0.32(1)$  (blue markers) and  $0.59(1)$  (light blue), respectively, prepared without RF

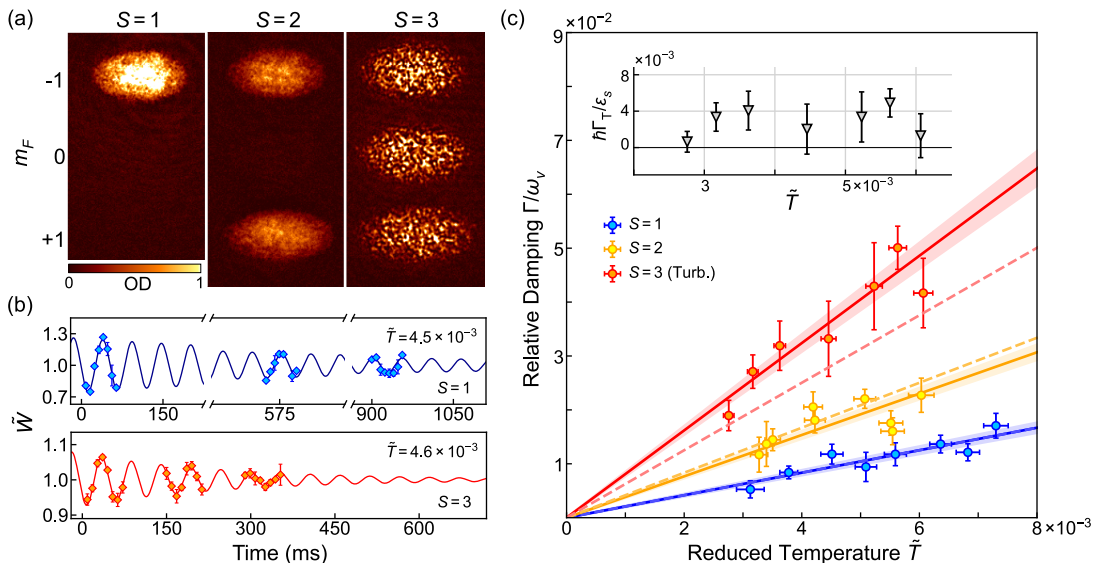


FIG. 3. Temperature dependence of the damping of collective oscillations of BECs. (a) Images of the three different types of BEC samples under investigation: a single-component ( $S = 1$ ) BEC and a two-component ( $S = 2$ ) BEC without turbulence, and a three-component turbulent BEC ( $S = 3$ ). The images were taken after Stern-Gerlach spin separation, showing the spin composition of the samples. (b) Free decay of the collective oscillations of the BECs with  $S = 1$  (upper) and  $S = 3$  (lower). The solid lines indicate damped sinusoidal curves,  $\tilde{W}(t) = 1 + Ae^{-\Gamma t} \sin(\omega_\nu t + \phi)$ , fitted to the data. (c) Relative damping rates  $\Gamma/\omega_\nu$  as functions of the reduced temperature  $\tilde{T}$  (see text) for  $S = 1, 2, 3$ . The solid lines represent linear fits to the data,  $\Gamma/\omega_\nu = A_\nu \tilde{T}$ , and the shaded regions indicate the  $1\sigma$  uncertainties of the fits. The dashed lines show the predictions of the thermal damping model for  $S = 2, 3$ , respectively, based on the measurement data for  $S = 1$ . The inset shows the excess damping rate  $\Gamma_T$  of the turbulent BEC, normalized by  $\varepsilon_s/\hbar$  where  $\varepsilon_s$  is the spin interaction energy at peak atomic density.

spin driving, and a turbulent BEC with  $\zeta_{\text{th}} = 0.57(1)$  (orange). Resonance behavior is evident in  $\tilde{A}$ , accompanied by a phase change of  $\pi$  in  $\phi$  as  $\omega_d$  increases. The resonance frequency  $\omega_\nu$  and the spectral width  $\Gamma$  are determined from the simultaneous fit of  $\tilde{A}(\omega_d) = \frac{A'\omega_\nu^2}{\sqrt{(\omega_d^2 - \omega_\nu^2)^2 + 4(\omega_d\Gamma)^2}}$  and  $\phi(\omega_d) = \frac{\pi}{2} + \tan^{-1}\left(\frac{\omega_d^2 - \omega_\nu^2}{2\Gamma\omega_d}\right) - \phi_0$  to the measurement data with  $A'$  and  $\phi_0$  being free parameters [36]. For ordinary BECs without turbulence, we obtain  $\Gamma/2\pi = 0.40(3)$  Hz and  $\Delta\omega_\nu/2\pi = (\omega_\nu - \omega_{\nu,0})/2\pi = 0.21(3)$  Hz for a low  $\zeta_{\text{th}}$ , and  $\Gamma/2\pi = 0.53(5)$  Hz and  $\Delta\omega_\nu/2\pi = 0.44(1)$  Hz for a high  $\zeta_{\text{th}}$ , where  $\omega_{\nu,0}/2\pi = 25.3$  Hz is the resonance frequency at zero temperature, calculated from the trap frequencies [35]. As  $\zeta_{\text{th}}$  increases, the resonance frequency shifts upward and the damping increases, consistent with previous studies of finite temperature effects [37–40].

The turbulent BEC exhibits more pronounced spectral broadening and a larger shift with  $\Gamma/2\pi = 1.1(1)$  Hz and  $\Delta\omega_\nu/2\pi = 1.6(3)$  Hz. The spectral width is more than twice that of an ordinary BEC with a comparable thermal fraction, suggesting that turbulence leads to enhanced damping. However, it is important to note that with RF driving both the thermal cloud and the turbulent BEC consist of three spin components with equal populations [3], resulting in a thermal temperature distinct from that of a single-component system having the

same thermal fraction. Thus, to validate the damping enhancement by turbulence, a more comprehensive analysis of the thermal damping effects is needed.

According to a theoretical description of Landau damping for low-lying collective excitations of a trapped BEC [24, 41], the damping rate  $\Gamma$  at temperature  $k_B T > \mu$  is given by

$$\frac{\Gamma}{\omega_\nu} = A_\nu \sqrt{n_0 a^3} \frac{k_B T}{\mu}, \quad (1)$$

where  $n_0$  is the maximum number density of the condensate,  $a$  is the scattering length, and  $k_B$  is the Boltzmann constant. The factor  $A_\nu$  is a dimensionless parameter determined by the spatial geometry of the trap and the characteristics of the collective mode  $\nu$ . When the number of spin components,  $S$ , in the thermal cloud increases, the population of thermal particles increases proportionally to  $S$ , while maintaining an identical momentum distribution at temperature  $T$ . Therefore, it is reasonable to expect that the damping rate would increase by the same factor as  $S$  [8, 42], assuming that the scattering property of the BEC remains the same across different spin components. We propose that  $A_\nu = S A_\nu^{(0)}$ , with  $A_\nu^{(0)}$  representing the value for a single-component system.

We investigate the temperature dependence of the damping rates for BECs with and without turbulence. The temperature is controlled by adjusting the final trap

depth of evaporation cooling, where the trapping frequencies of the final trap range from  $2\pi \times (4.4, 8.9, 420)$  Hz to  $2\pi \times (7.9, 16.3, 780)$  Hz, and correspondingly the thermal fraction changes approximately from 0.1 to 0.5 without turbulence and from 0.25 to 0.7 with turbulence. In order to avoid any issues arising from the relative oscillations of the thermal gas coexisting with the BECs [37–39, 43, 44], we measure the damping rate of the freely decaying oscillations of the BEC after a brief period of trap modulations this time. The modulation period is set to  $t_0 = 10 \frac{2\pi}{\omega_d}$  and the driving frequency is tuned to the red side of the resonance, further away from the closest thermal gas oscillating mode at  $2\omega_y$ . The damping rate  $\Gamma$  and the oscillation frequency  $\omega_\nu$  are determined from a damped sinusoidal function of  $\tilde{W}(t) = 1 + Ae^{-\Gamma t} \sin(\omega_\nu t + \phi)$  that fits the experimental data [Fig. 3(b)]. Furthermore, to verify the dependence of  $A_\nu$  on  $S$ , we conduct a parallel experiment with atomic samples having two spin components ( $S = 2$ ) [35], which are equal mixtures of the  $m_F = \pm 1$  components that are miscible [1, 45]. The field gradient is held below 1 mG/cm on the  $xy$  plane, preventing spin dragging effects caused by spatial separation of the spin components [47].

In Fig. 3(c), the relative damping rates  $\Gamma/\omega_\nu$  are shown for  $S = 1, 2, 3$ , plotted against the reduced temperature  $\tilde{T} \equiv k_B T \sqrt{n_0 a^3} / \mu$  [48]. The scattering length  $a$  varies for different spin components by up to 7% [49] but during the calculation of  $\tilde{T} (\propto a^{4/5})$ , we neglect such variations and use the value of  $a$  for the  $S = 1$  sample in the  $m_F = -1$  state. A linear relationship between  $\Gamma/\omega_\nu$  and  $\tilde{T}$  is observed as anticipated from Eq. (1). We determine the values of  $A_\nu$  by applying linear fits to the data sets, resulting in  $A_\nu = 2.1(1), 3.8(2),$  and  $8.1(4)$  for  $S = 1, 2, 3$ , respectively. The value of  $A_\nu$  for  $S = 1$ , that is,  $A_\nu^{(0)}$ , is more than two times smaller than the expected values from theory and experiment [24, 37], which might be due to the dimensional crossover effect for the tight confinement along the  $z$  direction [40, 51]. Notably, the value of  $A_\nu$  for samples with two spin components is found to be consistent with that of  $2A_\nu^{(0)}$  within the corresponding uncertainty range. This supports our assertion that the thermal damping rate is linearly proportional to the number of spin components.

In light of this finding, the observation that  $A_\nu > 3A_\nu^{(0)}$  for turbulent BECs ( $S = 3$ ) indicates that the BEC experiences enhanced damping above the expected thermal damping. Thus, we identify an excess damping as  $\Gamma_T = \Gamma - 3A_\nu^{(0)} \tilde{T} \omega_\nu$ , which we attribute to additional energy dissipation due to the presence of turbulence. The average value of  $\Gamma_T$  for our measurements over temperatures is approximately  $2\pi \times 0.2$  Hz. In the inset of Fig. 3(c), we plot  $\hbar \Gamma_T / \varepsilon_s$  with  $\varepsilon_s$  being the spin interaction energy at the peak atomic density, representing the turbulent kinetic energy scale of the system.

We now present a phenomenological interpretation of

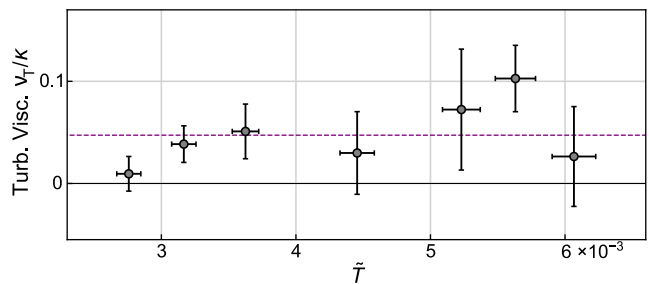


FIG. 4. Turbulent kinematic viscosity  $\nu_T$ , scaled by  $\kappa = h/m$ , for different  $\tilde{T}$ . The values of  $\nu_T$  were calculated from the excess damping rate  $\Gamma_T$  using Eq. (2). The horizontal dashed line indicates the average of the  $\nu_T$  values.

the excess damping observed with  $\Gamma_T$  using the turbulent viscosity  $\nu_T$ . In the conventional description of classical turbulence, Reynolds-averaged Navier-Stokes (RANS) equations are widely used, where the time-average effects of turbulence are encapsulated in  $\nu_T$ , providing a solvable model of the mean flow [1, 11, 12]. Following the reasoning of the RANS, we can introduce the kinematic viscosity  $\nu_T$  to our steady-state superfluid turbulence and derive the viscous damping rate  $\Gamma_T$  of collective oscillations, associated with  $\nu_T$  [13, 25]. For quadrupole oscillations with a mean velocity field of  $\mathbf{v}(\mathbf{r}, t) = (b_x x, b_y y, b_z z) \sin \omega_\nu t$ , the relationship between  $\Gamma_T$  and  $\nu_T$  is given by [35]

$$\Gamma_T = \frac{7\nu_T}{3\bar{R}^2} \frac{[3\sum_\alpha b_\alpha^2 - (\sum_\alpha b_\alpha)^2]}{\sum_\alpha b_\alpha^2 (\bar{\omega}/\omega_\alpha)^2} = \frac{7\nu_T}{3\bar{R}^2} F(\omega_\alpha, b_\alpha), \quad (2)$$

with  $\bar{R} = (R_x R_y R_z)^{1/3}$  and  $\bar{\omega} = (\omega_x \omega_y \omega_z)^{1/3}$ , where  $R_\alpha$  is the Thomas-Fermi (TF) radius of the condensate along the  $\alpha$  axis. The dimensionless parameter  $F$  characterizes a shear flow in the collective oscillation mode. In Fig. 4, we plot the values of  $\nu_T$  estimated from our experimental data using Eq. (2). The average value is obtained as  $\nu_T = 0.05(4) \times h/m$ . Intriguingly, the observed  $\nu_T$  is comparable in magnitude to the effective viscosity reported for turbulent superfluid  $^4\text{He}$  [53–55], which is associated with energy dissipation within turbulence rather than due to the mean shear flow.

A quantitative explanation of the increased damping observed in this study is currently beyond our understanding with regard to the steady-state turbulence generated in spinor BECs under spin driving. A comprehensive description of the energy transfer in this non-equilibrium BEC system is necessary, including the energy spectrum and cascade dynamics within the spin-superflow turbulence [7, 22], along with their alternation through interactions with the surrounding thermal component. This subject is intended for further exploration. Recent studies of plasma turbulence showed that Landau damping can either suppress turbulence [56] or serve as an energy dissipation mechanism to maintain it [57]. The



thermal change of the turbulent state could lead to temperature dependence of  $\Gamma_T$ , most likely implied in Fig. 4.

Finally, a noteworthy feature of our system is that, due to the oblate geometry of the sample, the turbulent flow exhibits mainly two-dimensional characteristics, whereas the mean flow of the collective modes is three-dimensional. This disparity could limit the use of the RANS method, which presupposes three-dimensional homogeneous isotropic turbulence. Previous research on classical turbulence driven by two-dimensional forcing demonstrated that enhancing the three-dimensional nature of turbulent flows can increase the eddy viscosity by suppressing the inverse energy cascade [58]. This suggests that probing the dimensional crossover presents an exciting direction for further investigation.

In summary, we have observed an enhancement in the damping of collective oscillations of BECs in the presence of turbulence. Investigating the viscous effects induced by turbulence through its coupling to collective excitations provides a novel framework for understanding the energy-transfer mechanisms and the hydrodynamic properties of superfluid turbulence. This work can extend to various collective excitation modes, particularly including a persistent monopole mode observed in spherically symmetric three-dimensional BECs [59].

This work was supported by the National Research Foundation of Korea (Grants No. NRF-2023R1A2C3006565, No. RS-2023-NR119928, and No. RS-2024-00413957).

- 
- [1] A. S. Monin and A. M. Obukhov, Basic laws of turbulent mixing in the surface layer of the atmosphere, *Contrib. Geophys. Inst. Acad. Sci. USSR* **151**, e187 (1954).
- [2] S. B. Pope, *Turbulent Flows*, (Cambridge University Press, Cambridge, 2000).
- [3] M. A. Leschziner and D. Drikakis, Turbulence modelling and turbulent-flow computation in aeronautics, *Aeronaut. J.* **106**, 349 (2002).
- [4] K. Bhide, K. Siddappaji, S. Abdallah, and K. Roberts, Improved supersonic turbulent flow characteristics using non-linear eddy viscosity relation in RANS and HPC-enabled LES, *Aerospace* **8**, 352 (2021).
- [5] Q. Chen, Comparison of different  $k-\varepsilon$  models for indoor air flow computations, *Numer. Heat Transf. B: Fundam.* **28**, 353 (1995).
- [6] H. Pu, C. K. Law, J. H. Eberly, and N. P. Bigelow, Coherent disintegration and stability of vortices in trapped Bose condensates, *Phys. Rev. A* **59**, 1533 (1999).
- [7] M. T. Noble, S. L. Ahlstrom, D. I. Bradley, E. A. Guise, R. P. Haley, S. Kafanov, G. R. Pickett, M. Poole, R. Schanen, T. Wilcox, A. J. Woods, D. E. Zmeev, and V. Tsepelin, Producing and imaging quantum turbulence via pair-breaking in superfluid  $^3\text{He-B}$ , *Phys. Rev. B* **105**, 174515 (2022).
- [8] L. Skrbek, D. Schmoranzer, Š. Midlik, and K. R. Sreenivasan, Phenomenology of quantum turbulence in superfluid helium, *Proc. Natl Acad. Sci. USA* **118**, e2018406118 (2021).
- [9] G. P. Bewley, M. S. Paoletti, K. R. Sreenivasan, and D. P. Lathrop, Characterization of reconnecting vortices in superfluid helium, *Proc. Natl. Acad. Sci. U.S.A.* **105**, 13707 (2008).
- [10] S. W. Seo, W. J. Kwon, S. Kang, and Y. Shin, Collisional dynamics of half-quantum vortices in a spinor Bose-Einstein condensate, *Phys. Rev. Lett.* **116**, 185301 (2016).
- [11] W. F. Vinen and J. J. Niemela, Quantum turbulence, *J. Low Temp. Phys.* **128**, 167 (2002).
- [12] N. Navon, A. L. Gaunt, R. P. Smith, and Z. Hadzibabic, Emergence of a turbulent cascade in a quantum gas, *Nature* **539**, 72 (2016).
- [13] D. F. Brewer and D. O. Edwards, Heat conduction by liquid helium II in capillary tubes. I: Transition to supercritical conduction, *Philos. Mag.* **6**, 775 (1961).
- [14] R. K. Childers and J. T. Tough, Eddy viscosity of turbulent superfluid  $^4\text{He}$ , *Phys. Rev. Lett.* **35**, 527 (1975).
- [15] S. Kashiwamura, K. Miyake, K. Yamada, and M. Yamaguchi, Effects of eddy viscosity of turbulent superfluid in capillary flows, *Physica B* **270**, 60 (1999).
- [16] M. E. Mossman, M. A. Hoefler, K. Julien, P. G. Kevrekidis, and P. Engels, Dissipative shock waves generated by a quantum-mechanical piston, *Nat. Commun.* **9**, 4665 (2018).
- [17] N. Andersson, T. Sidery, and G. L. Comer, Superfluid neutron star turbulence, *Mon. Not. R. Astron. Soc.* **381**, 747 (2007).
- [18] A. Melatos and B. Link, Pulsar timing noise from superfluid turbulence, *Mon. Not. R. Astron. Soc.* **437**, 21 (2014).
- [19] D. Hong, J. Lee, J. Kim, J. H. Jung, K. Lee, S. Kang, and Y. Shin, Spin-driven stationary turbulence in spinor Bose-Einstein condensates, *Phys. Rev. A* **108**, 013318 (2023).
- [20] J. H. Jung, J. Lee, J. Kim, and Y. Shin, Random spin textures in turbulent spinor Bose-Einstein condensates, *Phys. Rev. A* **108**, 043309 (2023).
- [21] J. Kim, J. Jung, J. Lee, D. Hong, and Y. Shin, Chaos-assisted turbulence in spinor Bose-Einstein condensates, *Phys. Rev. Res.* **6**, L032030 (2024).
- [22] K. Fujimoto and M. Tsubota, Spin-superflow turbulence in spin-1 ferromagnetic spinor Bose-Einstein condensates, *Phys. Rev. A* **90**, 013629 (2014).
- [23] L. D. Landau, On the vibrations of the electronic plasma, *J. Phys. USSR* **10**, 25 (1946).
- [24] P. O. Fedichev, G. V. Shlyapnikov, and J. T. M. Walraven, Damping of low-energy excitations of a trapped Bose-Einstein condensate at finite temperatures, *Phys. Rev. Lett.* **80**, 2269 (1998).
- [25] L. D. Landau and E. M. Lifshitz, *Fluid Mechanics: Landau and Lifshitz: Course of Theoretical Physics, Volume 6*, (Elsevier Science, Amsterdam, 1987).
- [26] F. G. Schmitt, About Boussinesq's turbulent viscosity hypothesis: historical remarks and a direct evaluation of its validity, *C. R. Méc.* **335**, 617 (2007).
- [27] Y. Kawaguchi and M. Ueda, Spinor Bose-Einstein condensates, *Phys. Rep.* **520**, 253 (2012).
- [28] S. W. Seo, S. Kang, W. J. Kwon, and Y. Shin, Half-quantum vortices in an antiferromagnetic spinor Bose-Einstein condensate, *Phys. Rev. Lett.* **115**, 015301 (2015).

- [29] M. Rautenberg and M. Gärttner, Classical and quantum chaos in a three-mode bosonic system, *Phys. Rev. A* **101**, 053604 (2020).
- [30] B. Evrard, A. Qu, J. Dalibard, and F. Gerbier, From many-body oscillations to thermalization in an isolated spinor gas, *Phys. Rev. Lett.* **126**, 063401 (2021).
- [31] C. Cao, E. Elliott, J. Joseph, H. Wu, J. Petricka, T. Schäfer, and J. E. Thomas, Universal quantum viscosity in a unitary Fermi gas, *Science* **331**, 58 (2011).
- [32] E. Vogt, M. Feld, B. Fröhlich, D. Pertot, M. Koschorreck, and M. Köhl, Scale invariance and viscosity of a two-dimensional Fermi gas, *Phys. Rev. Lett.* **108**, 070404 (2012).
- [33] S. Stringari, Collective excitations of a trapped Bose-condensed gas, *Phys. Rev. Lett.* **77**, 2360 (1996).
- [34] H. Heiselberg, Collective modes of trapped gases at the BEC-BCS crossover, *Phys. Rev. Lett.* **93**, 040402 (2004).
- [35] See Supplemental Material for experimental methods of sample preparation and imaging, details of the quadrupole modes of highly oblate condensates, and the derivation of Eq. (2) using the RANS equation.
- [36] For the experimental data,  $A' \approx 1.7$  and  $\phi_0 \approx 0.1\pi$ , attributed to systematic effects in the time-of-flight measurement.
- [37] D. S. Jin, M. R. Matthews, J. R. Ensher, C. E. Wieman, and E. A. Cornell, Temperature-dependent damping and frequency shifts in collective excitations of a dilute Bose-Einstein condensate, *Phys. Rev. Lett.* **78**, 764 (1997).
- [38] D. M. Stamper-Kurn, H.-J. Miesner, S. Inouye, M. R. Andrews, and W. Ketterle, Collisionless and hydrodynamic excitations of a Bose-Einstein condensate, *Phys. Rev. Lett.* **81**, 500 (1998).
- [39] R. Meppelink, S. B. Koller, J. M. Vogels, H. T. C. Stoof, and P. van der Straten, Damping of superfluid flow by a thermal cloud, *Phys. Rev. Lett.* **103**, 265301 (2009).
- [40] B. Yuen, I. J. M. Barr, J. P. Cotter, E. Butler, and E. A. Hinds, Enhanced oscillation lifetime of a Bose-Einstein condensate in the 3D/1D crossover, *New J. Phys.* **17**, 093041 (2015).
- [41] C. J. Pethick and H. Smith, *Bose-Einstein Condensation in Dilute Gases*, (Cambridge University Press, Cambridge, 2002).
- [42] A. B. Bhattacharjee, Damping in two-component Bose gas, *Mod. Phys. Lett. B* **28**, 1450029 (2014).
- [43] B. Jackson and E. Zaremba, Quadrupole collective modes in trapped finite-temperature Bose-Einstein condensates, *Phys. Rev. Lett.* **88**, 180402 (2002).
- [44] S. A. Morgan, M. Rusch, D. A. W. Hutchinson, and K. Burnett, Quantitative test of thermal field theory for Bose-Einstein condensates, *Phys. Rev. Lett.* **91**, 250403 (2003).
- [45] J. Stenger, S. Inouye, D. M. Stamper-Kurn, H.-J. Miesner, A. P. Chikkatur, and W. Ketterle, Spin domains in ground-state Bose-Einstein condensates, *Nature* **396**, 345 (1998).
- [46] F. Gerbier, A. Widera, S. Fölling, O. Mandel, and I. Bloch, Resonant control of spin dynamics in ultracold quantum gases by microwave dressing, *Phys. Rev. A* **73**, 041602 (2006).
- [47] R. A. Duine and H. T. C. Stoof, Spin drag in noncondensed Bose gases, *Phys. Rev. Lett.* **103**, 170401 (2009).
- [48] The sample temperature was estimated as  $k_B T = 0.94\hbar\bar{\omega}(N_{\text{th}}/S)^{1/3}$ , with  $N_{\text{th}}$  being the number of thermal atoms [41, 50]. Using TF approximation,  $\mu = \frac{\hbar\bar{\omega}}{2}(15N_c a/\bar{a})^{2/5}$  and  $n_0 = \mu \frac{m}{4\pi\hbar^2 a}$  with  $\bar{a} = \left(\frac{\hbar}{m\bar{\omega}}\right)^{1/2}$ .
- [49] S. Knoop, T. Schuster, R. Scelle, A. Trautmann, J. Appmeier, M. K. Oberthaler, E. Tiesinga and E. Tiemann, Feshbach spectroscopy and analysis of the interaction potentials of ultracold sodium, *Phys. Rev. A* **83**, 042704 (2011).
- [50] C. Frapolli, T. Zibold, A. Invernizzi, K. Jiménez-García, J. Dalibard, and F. Gerbier, Stepwise Bose-Einstein condensation in a spinor gas, *Phys. Rev. Lett.* **119**, 050404 (2017).
- [51] In our experiment,  $\mu/(\hbar\omega_z) \sim 2$ , while  $k_B T/(\hbar\omega_z)$  varied between 7 and 13.
- [52] G. M. Kavoulakis, C. J. Pethick, and H. Smith, Damping of hydrodynamic modes in a trapped Bose gas above the Bose-Einstein transition temperature, *Phys. Rev. A* **57**, 2938 (1998).
- [53] P. M. Walmsley and A. I. Golov, Quantum and quasiclassical types of superfluid turbulence, *Phys. Rev. Lett.* **100**, 245301 (2008).
- [54] D. E. Zmeev, P. M. Walmsley, A. I. Golov, P. V. E. McClintock, S. N. Fisher, and W. F. Vinen, Dissipation of quasiclassical turbulence in superfluid  $^4\text{He}$ , *Phys. Rev. Lett.* **115**, 155303 (2015).
- [55] S. Babuin, E. Varga, L. Skrbek, E. Lévêque, and P.-E. Roche, Effective viscosity in quantum turbulence: A steady-state approach, *Europhys. Lett.* **106**, 24006 (2014).
- [56] R. Ferrand, F. Sahraoui, D. Laveder, T. Passot, P. Sulem, and S. Galtier, Fluid energy cascade rate and kinetic damping: New insight from 3D Landau-fluid simulations, *Astrophys. J.* **923**, 122 (2021).
- [57] C. H. K. Chen, K. G. Klein, and G. G. Howes, Evidence for electron Landau damping in space plasma turbulence, *Nat. Commun.* **10**, 740 (2019).
- [58] M. Shats, D. Byrne, and H. Xia, Turbulence decay rate as a measure of flow dimensionality, *Phys. Rev. Lett.* **105**, 264501 (2010).
- [59] D. S. Lobser, A. E. S. Barentine, E. A. Cornell, and H. J. Lewandowski, Observation of a persistent non-equilibrium state in cold atoms, *Nat. Phys.* **11**, 1009 (2015).

## Supplemental Material

### Methods

#### *Sample preparation*

We prepared a thermal cloud of  $^{23}\text{Na}$  atoms in the  $|F = 1, m_F = -1\rangle$  state in an optical dipole trap (ODT) and applied evaporative cooling by reducing the trap depth to produce a Bose-Einstein condensate (BEC). The thermal fraction  $\zeta_{\text{th}}$  of the sample was controlled by adjusting the final value  $U_f$  of the trap depth. At our lowest temperatures, the typical number of atoms for the BEC was approximately  $7 \times 10^6$ . The atomic sample was held in the ODT for several seconds to relax residual motion before driving the collective excitations of the trapped BEC.

Depending on the target experiment, the atomic sample was transformed into a two-component system with  $|m_F = \pm 1\rangle$  states ( $S = 2$ ) or a turbulent system with  $|m_F = 0, \pm 1\rangle$  states ( $S = 3$ ). For the two-component system, first we transferred atoms to the  $|m_F = 0\rangle$  state using a rapid adiabatic passage with an RF magnetic field, with this followed by a pulse of a strong magnetic field gradient to purify the spin state. We then applied a  $\pi/2$  resonant RF magnetic pulse to form an equal mixture of the  $m_F = \pm 1$  components. After the preparation of the spin mixture, we irradiated a continuous microwave field detuned from the  $F = 1 \rightarrow F = 2$  transition to shift the quadratic Zeeman energy to a small negative value. This prevents the creation of atoms in the  $|F = 1, m_F = 0\rangle$  state via spin exchange processes, stabilizing the two-component system [1, 2].

The turbulent sample was prepared with the continuous application of the resonant RF field [3]. A steady turbulent state with an irregular spin texture was generated within 0.5 s, exhibiting equal populations of the three  $m_F = 0, \pm 1$  spin components. This turbulence is sustained by chaotic spin dynamics under RF spin driving [4], as detailed in Section B. Following 2 s of RF driving, we conducted the collective oscillation experiment while maintaining the RF spin driving. The BEC lifetime exceeded 30 s under RF driving ( $S = 3$ ) and was approximately 5 s under the microwave dressing ( $S = 2$ ), significantly longer than our measurement duration, which lasted for a few hundreds of ms.

The ODT was highly oblate such that the ratio of the trapping frequencies was  $\omega_x : \omega_y : \omega_z \approx 1 : 2 : 100$ . The trapping frequencies were measured by analyzing the dipole oscillations of a trapped BEC along the  $x$  and  $y$  directions and the parametric heating of trap modulations for the  $z$  axis.

#### *Imaging*

An absorption image of the sample was taken in the  $z$  direction after a time of flight of  $\tau = 18$  ms by releasing the trapping potential. In the case shown in Fig. 3(a), a magnetic field gradient pulse was applied during the expansion to separate the different spin components spatially. The number of atoms contained in the thermal gas,  $N_{\text{th}}$ , was estimated from a two-dimensional Gaussian distribution fit to the outer region of the cloud, and the number of condensed atoms  $N_c$  was determined from an image obtained by subtracting the fitted thermal profile from the original image. The thermal fraction is given by  $\zeta_{\text{th}} = N_{\text{th}}/N$  with  $N = N_c + N_{\text{th}}$ . The width  $W_\alpha(t)$  of the condensates along the  $\alpha$  axis ( $\alpha = x, y, z$ ) was determined by fitting the two-dimensional inverted parabola to the subtracted profile.

#### *Analysis of width oscillations*

The width  $W(t)$ , measured after the free expansion for  $\tau$ , is related with the in-situ width  $W_i(t)$  of the BEC as

$$W(t) = W_i(t) + \frac{dW_i(t)}{dt} \tau. \quad (\text{S1})$$

The second term accounts for the width change during the time of flight, owing to the oscillation velocity of the condensate. Here we neglect the expansion effect due to the mean-field energy, which is negligibly small along the  $y$  direction for our highly oblate geometry. When a trapped BEC oscillates as  $W_i(t) = W_{\text{eq}}(1 + A \sin(\omega t + \phi))$ , using Eq. (S1), the measured width is given by  $W(t) = W_{\text{eq}}(1 + \alpha_\tau A \sin(\omega t + \phi + \varphi_\tau))$  with  $\alpha_\tau = \sqrt{1 + (\omega\tau)^2}$  and  $\varphi_\tau = \tan^{-1}(\omega\tau)$ .  $W_{\text{eq}}$  denotes the in-situ width of the condensate at equilibrium.

In our data analysis, we used the normalized width  $\tilde{W} = W/W_{\text{eq}}$  to account for variations in the number of atoms in the sample. Using the relationship of  $W_{\text{eq}} \propto U_f^{-1/5} N_c^{1/5}$  in the Thomas-Fermi (TF) approximation, the equilibrium

width for a given  $N_c$  was estimated as  $W_{\text{eq}}(N_c) = \overline{W}_{\text{eq}}(N_c/\overline{N}_c)^{1/5}$ , where  $\overline{W}_{\text{eq}}$  and  $\overline{N}_c$  are the mean width and the mean number of atoms of the condensate, as determined by averaging tens of measurements without trap modulations.

### Stationary spin-superflow turbulence

Turbulence in a spin-1 BEC was induced by an RF magnetic field applied transversely to a uniform external field  $B_z$ . In a mean-field description, neglecting the spatial modes of the BEC and taking the rotating wave approximation, the local dynamics of the spin state  $\zeta = (\zeta_{+1}, \zeta_0, \zeta_{-1})^T$  of the BEC is governed by the following Hamiltonian per particle,

$$H_s = \hbar\delta f_z - \hbar\Omega f_x + q\zeta^\dagger f_z^2 \zeta + \varepsilon_s |\mathbf{f}|^2, \quad (\text{S2})$$

where  $\mathbf{f} = (f_x, f_y, f_z)$  are the spin operators of the spin-1 system and  $\mathbf{f} = \zeta^\dagger \mathbf{f} \zeta$  is the normalized spin vector with  $f_{x,y,z}$  representing the normalized magnetizations in  $x, y$ , and  $z$  directions, respectively. In addition,  $\delta = \omega - \omega_0$  is the frequency detuning of the RF magnetic field from the Larmor frequency  $\omega_0 = \frac{1}{2}\mu_B B_z/\hbar$  with  $\mu_B$  being the Bohr magneton,  $\Omega$  is the Rabi frequency of the RF field, and  $q$  denotes the quadratic Zeeman energy. The last term represents the spin interaction energy and  $\varepsilon_s > 0$  for antiferromagnetic interactions. In our experiment,  $\Omega = 2\pi \times 150$  Hz,  $q/\hbar = 47$  Hz, and  $\varepsilon_s/\hbar$  ranges from 37 Hz to 80 Hz for the peak atom density.

When the system is driven resonantly ( $\delta = 0$ ) and the energy scales of  $\hbar\Omega$ ,  $q$ , and  $\varepsilon_s$  are comparable, the spin dynamics of the Hamiltonian  $H_s$  becomes chaotic [5, 6]. Furthermore, in the experiment, the external magnetic field was slightly modulated due to field noises ( $\sim 1$  mG), which was found to enhance the chaoticity of the system, thus facilitating complete randomization of the spin state [4, 7]. Due to this chaotic spin dynamics, small spatial fluctuations in the wavefunction of the BEC, even when starting with a uniform spin texture, develop into complex spatial variations of the spin states, resulting in an irregular spin texture.

In a spinor BEC, a superflow is associated not only with the spatial variations of the superfluid phase  $\varphi$  but also with those of  $\zeta$ , i.e., the spin texture [8]. The superfluid velocity  $\mathbf{v}$  and corresponding vorticity are given by

$$\begin{aligned} \mathbf{v} &= \frac{\hbar}{m} (\nabla\varphi - i\zeta^\dagger \nabla\zeta), \\ \nabla \times \mathbf{v} &= -\frac{i\hbar}{m} \nabla\zeta^\dagger \times \nabla\zeta, \end{aligned} \quad (\text{S3})$$

where  $m$  is the particle mass. Therefore, when the spin texture is continuously driven to be randomized due to chaotic spin dynamics, the associated turbulent flow in the BEC is sustained [4].

### Quadrupole modes of highly oblate condensates

In this section, we briefly describe the collective quadrupole excitation modes of a BEC trapped in a harmonic potential, following earlier works [9, 10]. Based on the time-dependent Gross-Pitaevskii equation for a macroscopic wavefunction of condensate  $\psi(\mathbf{r}, t) \equiv \sqrt{n(\mathbf{r}, t)}e^{i\varphi(\mathbf{r}, t)}$ , where  $n$  is the local particle density of the condensate, the equations of motion for the BEC are given by

$$\frac{\partial n}{\partial t} + \nabla \cdot (n\mathbf{v}) = 0, \quad (\text{S4})$$

$$\frac{\partial \mathbf{v}}{\partial t} + (\mathbf{v} \cdot \nabla)\mathbf{v} = -\frac{1}{m} \nabla \left( V_{\text{ext}} + gn - \frac{\hbar^2}{2m} \frac{\nabla^2 \sqrt{n}}{\sqrt{n}} \right), \quad (\text{S5})$$

where  $\mathbf{v} = \frac{\hbar}{m} \nabla\varphi$  is the superfluid velocity field,  $g$  represents the interaction strength, and  $V_{\text{ext}}(\mathbf{r}) = \frac{1}{2}m \sum_{\alpha} \omega_{\alpha}^2 r_{\alpha}^2$  is the external harmonic potential, with  $r_{\alpha}$  representing the coordinates along the  $\alpha$  axis ( $\alpha = x, y, z$ ). Eq. (S4) is the continuity equation for the conservation of the particle number and Eq. (S5) is referred to as the quantum Navier-Stokes equation (or the Euler equation for a superfluid). Using the Thomas-Fermi (TF) approximation, the last term of Eq. (S5), called the quantum pressure, is neglected and the equilibrium density profile of the BEC is given as  $n_0(\mathbf{r}) = \max[\frac{\mu - V_{\text{ext}}(\mathbf{r})}{g}, 0]$ , where  $\mu$  is the chemical potential of the condensate. Note that this approximation is not reliable near the boundary region at a low particle density.



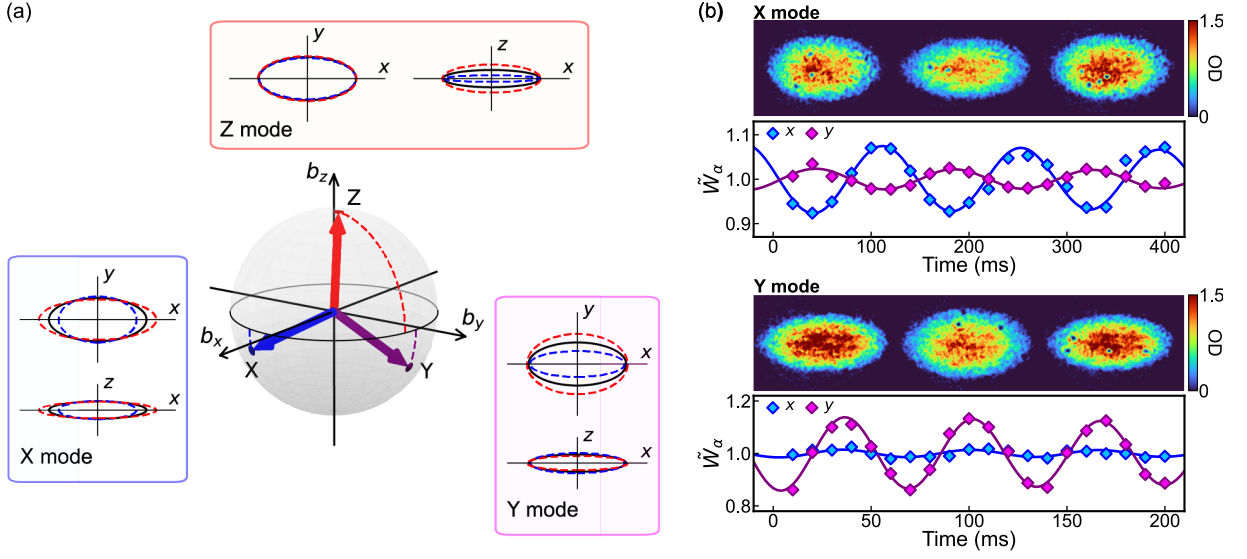


FIG. S1. (a) Quadrupole oscillation modes for an oblate BEC with trapping frequencies  $\omega_x < \omega_y < \omega_z$ . The oscillatory motion is characterized by  $(b_x, b_y, b_z)$ , as shown in Eq. (S9), and the three modes are denoted by X, Y, and Z, respectively, corresponding to the dominant oscillation axis. The variation in the density profile in the  $xy$  and  $xz$  planes for each mode is presented. (b) and (c) Experimental observation of the quadrupole oscillations of BECs. BEC samples with  $S = 1$  were prepared at our lowest temperatures and the X or Y mode was selectively excited by short trap modulations at a frequency slightly red-detuned from resonance. The upper panels in (b) and (c) display time-of-flight images of BECs oscillating in the X and Y modes, respectively, at different hold times. The lower panels show the time evolution of the normalized condensate widths in the  $x$  and  $y$  directions, respectively. Solid lines indicate damped sinusoidal fits to the experimental data.

To derive the low-lying collective excitation modes of the BEC, we consider a small variation of the number density from its equilibrium value, which oscillates in time with the angular frequency  $\omega$ . By replacing the number density with  $n = n_0(\mathbf{r}) + \delta n(\mathbf{r}) \cos \omega t$  in Eqs. (S4) and (S5), we obtain, to the linear order of  $\delta n$ ,

$$\omega^2 \delta n = \frac{1}{m} [\nabla V_{\text{ext}} \cdot \nabla \delta n - (\mu - V_{\text{ext}}) \nabla^2 \delta n], \quad (\text{S6})$$

and the ansatz  $\delta n(\mathbf{r}) = b_0 + \sum_{\alpha} b_{\alpha} r_{\alpha}^2$  for quadrupole excitations leads to the characteristic equations

$$(2\omega_{\alpha}^2 - \omega^2) b_{\alpha} + \omega_{\alpha}^2 \sum_{\beta=x,y,z} b_{\beta} = 0, \quad (\text{S7})$$

$$\omega^2 b_0 + \frac{2\mu}{m} \sum_{\alpha} b_{\alpha} = 0. \quad (\text{S8})$$

Eq. (S7) presents three independent sets of solutions for  $(\omega, b_{\alpha})$ , corresponding to different modes of quadrupole excitation. From the linearized form of Eq. (S4) for small values of  $\delta n$  and  $\mathbf{v}$ , the velocity field in the oscillating BEC is given by

$$\mathbf{v}(\mathbf{r}, t) = -\frac{2g}{m\omega} (b_x x, b_y y, b_z z) \sin \omega t. \quad (\text{S9})$$

The three quadrupole excitation modes for an oblate trapping potential with  $\omega_x < \omega_y < \omega_z$  are depicted in Fig. S1(a), which we refer to as the X, Y, and Z modes, respectively, indicating the axis of dominant width oscillations. In the X (Y) mode, the condensate exhibits out-of-phase (in-phase) width oscillations along the  $x$  and  $y$  directions. We experimentally identified the two quadrupole oscillation modes by applying trap modulations at various frequencies and measuring the width oscillations of the condensate along the  $x$  and  $y$  directions [Figs. S1(b) and S1(c)]. For our samples at the lowest temperature  $\zeta_{\text{th}} < 0.1$  and  $S = 1$ , the oscillation frequencies were measured and found to be  $\omega/2\pi = 7.0(1)$  Hz and  $15.0(2)$  Hz for the X and Y modes, respectively, which are in good agreement with the predicted values of 7.0 Hz and 14.7 Hz from Eq. (S7) with the trapping frequencies of  $(\omega_x, \omega_y, \omega_z)/2\pi = (4.4, 8.9, 415)$  Hz.

### Quantum Reynolds-Averaged Navier-Stokes equation

Reynolds-averaged Navier-Stokes (RANS) equations are a widely used approach for modeling turbulent flows [11]. They are derived by decomposing the instantaneous quantities, such as the velocity and pressure, into mean and fluctuating components, allowing the effects of turbulence to be captured in a time-averaged manner.

Let us consider the quantum Navier-Stokes equation in Eq. (S5) and a situation in which the velocity  $\mathbf{v}$  can be decomposed into the mean velocity  $\bar{\mathbf{v}}$  and the fluctuating part  $\mathbf{v}'$  under the assumption of isotropic and homogeneous turbulence. Taking the time-averaged form of the equation, where the first-order fluctuation terms cancel out, we obtain the RANS equation as

$$\frac{\partial \bar{v}_\alpha}{\partial t} + (\bar{\mathbf{v}} \cdot \nabla) \bar{v}_\alpha = -\frac{1}{m} \frac{\partial p}{\partial r_\alpha} - \frac{1}{\bar{n}} \sum_\beta \frac{\partial}{\partial r_\beta} \overline{nv'_\alpha v'_\beta}, \quad (\text{S10})$$

where  $p = V_{\text{ext}} + g\bar{n}$  is the effective pressure, neglecting the quantum pressure. The upper bar indicates the mean over time averaging. The last term,  $\overline{nv'_\alpha v'_\beta}$ , is known as the Reynolds stress tensor and its value cannot be determined a priori, a situation commonly termed the turbulence closure problem. In an analogy to the molecular viscosity that arises from molecular motion in a gas, the Boussinesq hypothesis was proposed [12], stating that Reynolds stresses can be modeled as proportional to the mean strain rate and thus introduce turbulent viscosity in the mean flow motion. According to this model, the Reynolds stress tensor is approximated as

$$-\overline{nv'_\alpha v'_\beta} = \bar{n}\nu_T \sigma_{\alpha\beta} - \frac{2}{3} k \delta_{\alpha\beta}, \quad (\text{S11})$$

where  $\nu_T$  is the turbulent viscosity,  $\sigma_{\alpha\beta} = \frac{\partial \bar{v}_\alpha}{\partial r_\beta} + \frac{\partial \bar{v}_\beta}{\partial r_\alpha} - \frac{2}{3} \delta_{\alpha\beta} \nabla \cdot \bar{\mathbf{v}}$  is the traceless mean strain rate tensor, and  $k = \frac{1}{2} \sum_\alpha \overline{nv_\alpha'^2}$  is the turbulent kinetic energy.

### Turbulent damping of collective oscillations

Integrating the turbulent viscosity from Eq. (S11) into the RANS equation, the linearized equation of motion for a small variation of the mean number density,  $\delta\bar{n}$ , remains identical to Eq. (S6). This means that, despite the perturbation of the turbulent viscosity, the quadrupole excitation modes for a trapped BEC continue to hold for the averaged number density and velocity field, and their oscillation frequency and profile  $(\omega, b_\alpha)$  remain consistent with those derived in Section C.

The primary effect of turbulent viscosity is the dissipation of energy from the quadrupole oscillations. The total mechanical energy  $E$  for the collective oscillations with respect to the equilibrium state is twice the time average of the kinetic energy  $E_{kin}(t) = \int d\mathbf{r} \frac{1}{2} m \bar{n}(\mathbf{r}, t) \bar{v}^2(\mathbf{r}, t)$  [13] and up to the linear order of  $\delta\bar{n}$  and  $\bar{\mathbf{v}}$ , it is given by

$$E = \int d\mathbf{r} \left[ \frac{1}{2} m n_0(\mathbf{r}) \sum_\alpha \left( \frac{2g}{m\omega} \right)^2 b_\alpha^2 r_\alpha^2 \right]. \quad (\text{S12})$$

The rate of energy dissipation due to viscosity is given by

$$\dot{E}(t) = \int d\mathbf{r} \sum_{\alpha,\beta} m \bar{v}_\alpha \frac{\partial}{\partial r_\beta} \left( \bar{n}\nu_T \sigma_{\alpha\beta} - \frac{2}{3} k \delta_{\alpha\beta} \right). \quad (\text{S13})$$

To calculate the damping rate of our quadrupole mode, assuming that the amplitude of the quadrupole oscillation does not significantly change over an oscillation period, the mean energy dissipation rate is expressed as [14]

$$\langle \dot{E} \rangle_T = - \int d\mathbf{r} \left[ \frac{1}{2} m n_0(\mathbf{r}) \nu_T \sum_{\alpha,\beta=1}^3 \langle \sigma_{\alpha\beta}^2(\mathbf{r}, t) \rangle_T \right], \quad (\text{S14})$$

where  $\langle \dots \rangle_T$  denotes the time average over a period of one oscillation.

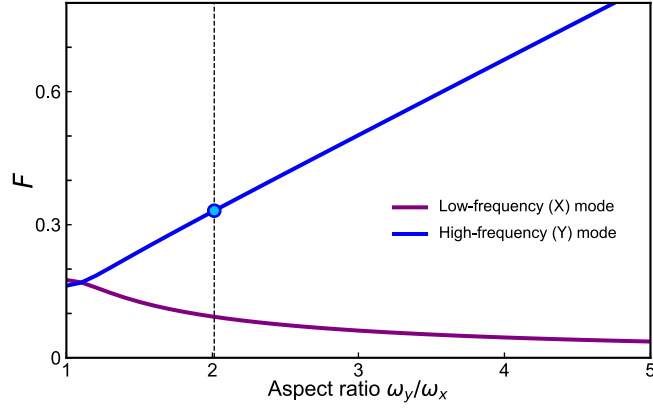


FIG. S2. Characteristic strain values  $F(\omega_\alpha, b_\alpha)$  for the X (low-frequency) and Y (high-frequency) modes are plotted as functions of the trap aspect ratio  $\lambda = \omega_y/\omega_x$ . The parameter  $\omega_z$  and  $\sqrt{\omega_x\omega_y}$  are kept constant in the experiment. The dashed vertical line indicates the experimental trap condition, where the Y mode (blue circle) exhibits stronger shear stress than the X mode.

The amplitude decay rate  $\Gamma_T$  of the collective oscillations is estimated as  $\Gamma_T = -\frac{1}{2}\langle\dot{E}\rangle_T/E$  and for the velocity field  $\bar{v}$  of the quadrupole mode in Eq. (S9), the damping rate is given by

$$\Gamma_T = \frac{7\nu_T}{3\bar{R}^2} \frac{[3\sum_\alpha b_\alpha^2 - (\sum_\alpha b_\alpha)^2]}{\sum_\alpha b_\alpha^2(\bar{\omega}/\omega_\alpha)^2} = \frac{7\nu_T}{3\bar{R}^2} F(\omega_\alpha, b_\alpha), \quad (\text{S15})$$

with  $\bar{R} = (R_x R_y R_z)^{1/3}$  and  $\bar{\omega} = (\omega_x \omega_y \omega_z)^{1/3}$ , where  $R_\alpha$  denotes the TF radius along the  $\alpha$  axis. We note that  $F(\omega_\alpha, b_\alpha)$  is a dimensionless parameter that is determined by the trapping frequencies and the collective oscillation profile, representing the degree of shear stress in the given collective excitation mode.

In Fig. S2, we plot the values  $F$  for the X and Y quadrupole modes as functions of the aspect ratio of the transverse trapping frequencies  $\lambda = \omega_y/\omega_x$ . In general, the Y mode, which exhibits in-phase oscillation on the  $xy$  plane, displays stronger shear stress than the X mode with out-of-phase oscillations, due to the motion along the  $z$  direction. This analysis suggests that the dependence of  $\Gamma_T$  on the trap geometry and collective modes could provide experimental validation of our turbulent viscosity model for the damped oscillations of a trapped BEC with turbulence.

- 
- [S1] F. Gerbier, A. Widera, S. Fölling, O. Mandel, and I. Bloch, Resonant control of spin dynamics in ultracold quantum gases by microwave dressing, *Phys. Rev. A* **73**, 041602 (2006).
  - [S2] S. W. Seo, S. Kang, W. J. Kwon, and Y. Shin, Half-quantum vortices in an antiferromagnetic spinor Bose-Einstein condensate, *Phys. Rev. Lett.* **115**, 015301 (2015).
  - [S3] D. Hong, J. Lee, J. Kim, J. H. Jung, K. Lee, S. Kang, and Y. Shin, Spin-driven stationary turbulence in spinor Bose-Einstein condensates, *Phys. Rev. A* **108**, 013318 (2023).
  - [S4] J. Kim, J. Jung, J. Lee, D. Hong, and Y. Shin, Chaos-assisted turbulence in spinor Bose-Einstein condensates, *Phys. Rev. Res.* **6**, L032030 (2024).
  - [S5] M. Rautenberg and M. Gärtner, Classical and quantum chaos in a three-mode bosonic system, *Phys. Rev. A* **101**, 053604 (2020).
  - [S6] B. Evrard, A. Qu, J. Dalibard, and F. Gerbier, From many-body oscillations to thermalization in an isolated spinor gas, *Phys. Rev. Lett.* **126**, 063401 (2021).
  - [S7] J. H. Jung, J. Lee, J. Kim, and Y. Shin, Random spin textures in turbulent spinor Bose-Einstein condensates, *Phys. Rev. A* **108**, 043309 (2023).
  - [S8] Y. Kawaguchi and M. Ueda, Spinor Bose-Einstein condensates, *Phys. Rep.* **520**, 253 (2012).
  - [S9] S. Stringari, Collective excitations of a trapped Bose-condensed gas, *Phys. Rev. Lett.* **77**, 2360 (1996).
  - [S10] H. Heiselberg, Collective modes of trapped gases at the BEC-BCS crossover, *Phys. Rev. Lett.* **93**, 040402 (2004).
  - [S11] S. B. Pope, *Turbulent Flows*, (Cambridge University Press, Cambridge, 2000).
  - [S12] F. G. Schmitt, About Boussinesq's turbulent viscosity hypothesis: historical remarks and a direct evaluation of its validity, *C. R. Méc.* **335**, 617 (2007).
  - [S13] G. M. Kavoulakis, C. J. Pethick, and H. Smith, Damping of hydrodynamic modes in a trapped Bose gas above the Bose-Einstein transition temperature, *Phys. Rev. A* **57**, 2938 (1998).

[S14] L. D. Landau and E. M. Lifshitz, *Fluid Mechanics: Landau and Lifshitz: Course of Theoretical Physics, Volume 6*, (Elsevier Science, Amsterdam, 2013).